

9-1-2008

Cancellation of Spurious Arrivals in Green's Function Extraction

Kasper van Wijk
Boise State University

Cancellation of spurious arrivals in Green's function extraction and the generalized optical theorem

Roel Snieder,^{1,*} Kasper van Wijk,² Matt Haney,³ and Rodney Calvert^{4,†}

¹Center for Wave Phenomena and Department of Geophysics, Colorado School of Mines, Golden, Colorado, 80401, USA

²Physical Acoustics Laboratory and Department of Geosciences, Boise State University, Boise, Idaho 83725, USA

³USGS Alaska Volcano Observatory, Anchorage, Alaska 99508, USA

⁴Shell International E&P, Houston, Texas 77001, USA

(Received 21 January 2008; published 18 September 2008)

The extraction of the Green's function by cross correlation of waves recorded at two receivers nowadays finds much application. We show that for an arbitrary small scatterer, the cross terms of scattered waves give an unphysical wave with an arrival time that is independent of the source position. This constitutes an apparent inconsistency because theory predicts that such spurious arrivals do not arise, after integration over a complete source aperture. This puzzling inconsistency can be resolved for an arbitrary scatterer by integrating the contribution of all sources in the stationary phase approximation to show that the stationary phase contributions to the source integral cancel the spurious arrival by virtue of the generalized optical theorem. This work constitutes an alternative derivation of this theorem. When the source aperture is incomplete, the spurious arrival is not canceled and could be misinterpreted to be part of the Green's function. We give an example of how spurious arrivals provide information about the medium complementary to that given by the direct and scattered waves; the spurious waves can thus potentially be used to better constrain the medium.

DOI: [10.1103/PhysRevE.78.036606](https://doi.org/10.1103/PhysRevE.78.036606)

PACS number(s): 43.20.+g, 03.65.Nk

I. INTRODUCTION

In recent years the extraction of the Green's function from field fluctuations has received considerable attention. This technique is described in recent tutorials [1,2], and is in the seismic community known as *seismic interferometry*. The Green's function can be retrieved by cross correlating the fields recorded at two receivers. This approach can be used to extract the impulse response from field fluctuations from thermal noise exciting elastic waves [3], from oceanic noise exciting surface waves [4,5], from turbulent flow over an airfoil [6], from chaotic earthquake signals [7,8], from industrial noise propagating in the subsurface [9], or from skeletal muscle noise [10]. Alternatively, one can use controlled sources. In this case the advantage of extracting the impulse response from cross correlation lies in the removal of the imprint of medium complexity between the sources and the receivers [11], or in a more optimal illumination of the target [12,13].

Even though the theory of Green's function extraction is well developed and numerous applications have been implemented, there are puzzling open questions; this work presents one of those questions. The Green's function G can be extracted by cross-correlating field fluctuations in two locations \mathbf{r}_A and \mathbf{r}_B . In the frequency domain expression (21) of Ref. [14] is

$$\oint \frac{1}{\rho(\mathbf{r})} [G^*(\mathbf{r}_B, \mathbf{r}) \nabla G(\mathbf{r}_A, \mathbf{r}) - G(\mathbf{r}_A, \mathbf{r}) \nabla G^*(\mathbf{r}_B, \mathbf{r})] \cdot \hat{\mathbf{n}} dS = 2i \operatorname{Im}(G(\mathbf{r}_A, \mathbf{r}_B)), \quad (1)$$

where $\rho(\mathbf{r})$ is the density, $\hat{\mathbf{n}}$ is the normal outward on the integration surface, and Im denotes the imaginary part. For sources far from the receivers ($r \gg r_{(A,B)}$) the Green's function satisfies a radiation boundary condition, so that for a spherical surface with a normal vector in the radial direction $\nabla G(\mathbf{r}_{A,B}, \mathbf{r}) = ikG(\mathbf{r}_{A,B}, \mathbf{r})\hat{\mathbf{n}}$. Using this radiation boundary condition, and reciprocity [$G(\mathbf{r}_1, \mathbf{r}_2) = G(\mathbf{r}_2, \mathbf{r}_1)$] gives, for a constant wave number k and density on the surface,

$$\oint G(\mathbf{r}_A, \mathbf{r}) G^*(\mathbf{r}_B, \mathbf{r}) dS = -\frac{\rho}{2ik} [G(\mathbf{r}_A, \mathbf{r}_B) - G^*(\mathbf{r}_B, \mathbf{r}_A)]. \quad (2)$$

Expression (2) is applicable for the case of acoustic waves treated here. By replacing ρ/k in the right hand side by $k\hbar^2/m$, the analysis is equally applicable to quantum mechanics [15]. The superposition of the Green's function and its complex conjugate in the right hand side, corresponds, in the time domain, to the superposition of the causal and acausal Green's function. This reflects the well-known fact that the cross correlation leads to the superposition of the causal Green's function and its acausal counterpart (e.g., [16,17]). Expression (2) forms the basis for the Green's function retrieval from the cross correlation of waves excited by uncorrelated sources on a closed surface surrounding the observation points [16]. A similar relation is valid for open systems where the surface integration needs to be replaced by an integration over all angles of incidence [18]. Expression (2) contains a surface integral. The counterpart of this expression for general linear systems that are not invariant for time reversal contains a volume integral as well [15,19,20].

According to Eq. (2), the Green's function can be found by cross correlating the waves excited by sources on a closed surface. We present in Sec. II a puzzle that suggests that

*rsnieder@mines.edu

†Deceased.

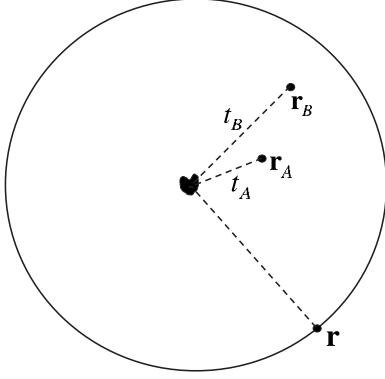


FIG. 1. The correlation of scattered waves traveling to points \mathbf{r}_A and \mathbf{r}_B and the times t_A and t_B used in the discussion of the spurious arrivals.

unphysical arrivals arise from expression (2). We solve this puzzle in Sec. III, and illustrate this with a numerical example in the subsequent section. This work is not only of academic interest, we discuss the implications for practical applications of the Green's function retrieval in the Conclusion. Details of the employed stationary phase approximations are shown in the Appendix.

II. PUZZLING APPARENT INCONSISTENCY

We consider the special case of an isolated scatterer as shown in Fig. 1 with scattering amplitude $f_k(\hat{\mathbf{n}}, \hat{\mathbf{n}}')$ for incident waves with wave number k traveling in the $\hat{\mathbf{n}}'$ direction that are scattered in the $\hat{\mathbf{n}}$ direction. The subsequent analysis is in the frequency domain, and, because k is constant at a fixed frequency, we suppress the subscript k in the following.

To introduce the puzzle we consider, for the moment, scattering by an acoustic sphere with a radius much smaller than a wavelength, for such a scatterer the phase is independent of frequency and of scattering angle [21]. The scattered waves travel over a time t_A from the scatterer to the receiver at \mathbf{r}_A and in a time t_B from the scatterer to the receiver at \mathbf{r}_B . The Green's function contains a scattered wave that propagates from \mathbf{r}_A via the scatterer to \mathbf{r}_B . The arrival time of this scattered wave is given by the *sum* $t_A + t_B$. The cross correlation of these scattered waves gives, in the time domain, a wave arriving at the *difference* of these arrival times. Note that this time difference is the same for any source location \mathbf{r} . The correlation of the scattered waves in expression (2) thus gives a wave arriving at a time $t_A - t_B$ at which no physical wave arrives. We call such a wave a *spurious arrival*. Since this arrival has the same travel time for all source positions \mathbf{r} it appears that there is no reason why this arrival vanishes by averaging over all source positions. In the following section we investigate this apparent inconsistency by a detailed evaluation of the integral in expression (2).

The situation sketched here applies equally well to an arbitrary scatterer, but in that case the phase of the scattering amplitude may depend on frequency. In that case the correlation does not give a wave arriving at a constant time $t_A - t_B$, but the cross correlation of the scattered waves still has

a phase that is determined by the phase difference of the scattered waves rather than by their sum. In the following we assume a general scatterer that may have a finite extent and does not need to be either isotropic or weak.

III. STATIONARY PHASE EVALUATION OF THE INTEGRAL

In our analysis we follow the treatment of van der Hulst [22] and assume sources far away ($r \gg r_{A,B}$), consistent with our assumption in Eq. (2). This makes it possible to evaluate the surface integral with the stationary phase analysis. The stationary phase approximation is exact in the limit $r \rightarrow \infty$. The waves excited by a point source at \mathbf{r} recorded at locations $\mathbf{r}_{A,B}$ is given by

$$G(\mathbf{r}_A, \mathbf{r}) = -\frac{\rho}{4\pi} \frac{e^{ik|\mathbf{r}-\mathbf{r}_A|}}{|\mathbf{r}-\mathbf{r}_A|} - \frac{\rho}{4\pi} \frac{e^{ikr}}{r} f(\hat{\mathbf{r}}_A, -\hat{\mathbf{r}}) \frac{e^{ikr_A}}{r_A}, \quad (3)$$

$$G(\mathbf{r}_B, \mathbf{r}) = -\frac{\rho}{4\pi} \frac{e^{ik|\mathbf{r}-\mathbf{r}_B|}}{|\mathbf{r}-\mathbf{r}_B|} - \frac{\rho}{4\pi} \frac{e^{ikr}}{r} f(\hat{\mathbf{r}}_B, -\hat{\mathbf{r}}) \frac{e^{ikr_B}}{r_B}. \quad (4)$$

The cross correlation of these fields corresponds, in the frequency domain, to

$$\begin{aligned} & \oint G(\mathbf{r}_A, \mathbf{r}) G^*(\mathbf{r}_B, \mathbf{r}) dS \\ &= \underbrace{\frac{\rho^2}{(4\pi)^2} \oint \frac{\exp[ik(|\mathbf{r}-\mathbf{r}_A| - |\mathbf{r}-\mathbf{r}_B|)]}{|\mathbf{r}-\mathbf{r}_A||\mathbf{r}-\mathbf{r}_B|} dS}_{T1} \\ &+ \underbrace{\frac{\rho^2}{(4\pi)^2} \oint \frac{\exp[ik(|\mathbf{r}-\mathbf{r}_A| - r - r_B)]}{|\mathbf{r}-\mathbf{r}_A| r r_B} f^*(\hat{\mathbf{r}}_B, -\hat{\mathbf{r}}) dS}_{T2} \\ &+ \underbrace{\frac{\rho^2}{(4\pi)^2} \oint \frac{\exp[-ik(|\mathbf{r}-\mathbf{r}_B| - r - r_A)]}{|\mathbf{r}-\mathbf{r}_B| r r_A} f(\hat{\mathbf{r}}_A, -\hat{\mathbf{r}}) dS}_{T3} \\ &+ \underbrace{\frac{\rho^2}{(4\pi)^2} \oint \frac{\exp[ik(r_A - r_B)]}{r^2 r_A r_B} f(\hat{\mathbf{r}}_A, -\hat{\mathbf{r}}) f^*(\hat{\mathbf{r}}_B, -\hat{\mathbf{r}}) dS}_{T4} \end{aligned} \quad (5)$$

The term $T1$ represents the cross terms of the direct waves at the two receivers, the terms $T2$ and $T3$ represent cross terms of the direct wave and a scattered wave, while the term $T4$ accounts for the cross term of the scattered waves. Note that the latter term contains a phase factor $\exp[ik(r_A - r_B)]$ for every integration point, hence it is this term that corresponds, in the time domain, to the spurious arrival discussed in Sec. II.

We carry out the surface integrals using a system of spherical coordinates as shown in Fig. 2. Without loss of generality we use a coordinate system with the scatterer cen-

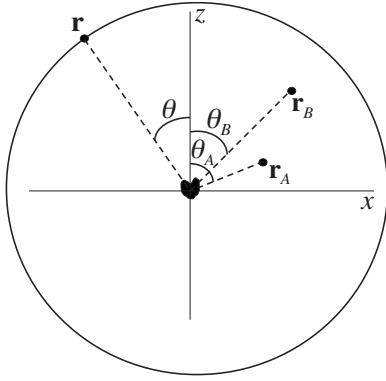


FIG. 2. Definition of geometric variables.

tered on the origin and where the points \mathbf{r}_A and \mathbf{r}_B are located in the (x, z) plane with $x_B > x_A$ and $z_B > z_A$. In this coordinate system,

$$\mathbf{r}_A = r_A \begin{pmatrix} \sin \theta_A \\ 0 \\ \cos \theta_A \end{pmatrix}, \quad \mathbf{r}_B = r_B \begin{pmatrix} \sin \theta_B \\ 0 \\ \cos \theta_B \end{pmatrix}, \quad \mathbf{r} = \begin{pmatrix} \sin \theta \cos \varphi \\ \sin \theta \sin \varphi \\ \cos \theta \end{pmatrix}. \quad (6)$$

For sources located far away ($r \gg r_{A,B}$), this gives to first order in $r_{A,B}/r$,

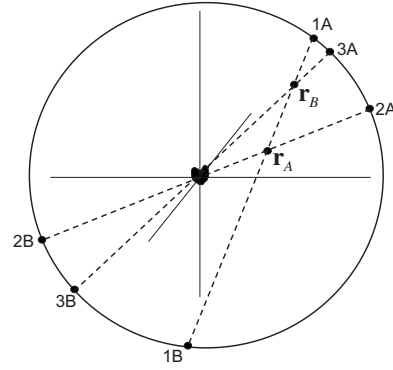


FIG. 3. Stationary points in the surface integral of different terms.

$$|\mathbf{r} - \mathbf{r}_{A,B}| = r - r_{A,B}(\cos \varphi \sin \theta \sin \theta_{A,B} + \cos \theta \cos \theta_{A,B}). \quad (7)$$

We use this approximation in the exponents of expression (5) while we replace $|\mathbf{r} - \mathbf{r}_{A,B}|$ in the denominators by r . With these replacements the incoming waves effectively are plane waves, which make our analysis applicable for the treatment of the extraction of the Green's function from incoming plane waves [18] as well. The surface integral is related to an integration over solid angle by the relation $dS = r^2 d\Omega$. Making these simplifications, expression (5) reduces to

$$\oint G(\mathbf{r}_A, \mathbf{r}) G^*(\mathbf{r}_B, \mathbf{r}) dS = \underbrace{\frac{\rho^2}{(4\pi)^2} \oint \exp(ikL_1) d\Omega}_{T1} + \underbrace{\frac{\rho^2}{(4\pi)^2} \oint \frac{\exp(ikL_2)}{r_B} f^*(\hat{\mathbf{r}}_B, -\hat{\mathbf{r}}) d\Omega}_{T2} + \underbrace{\frac{\rho^2}{(4\pi)^2} \oint \frac{\exp(-ikL_3)}{r_A} f(\hat{\mathbf{r}}_A, -\hat{\mathbf{r}}) d\Omega}_{T3} + \underbrace{\frac{\rho^2}{(4\pi)^2} \frac{\exp[ik(r_A - r_B)]}{r_A r_B} \oint f(\hat{\mathbf{r}}_A, -\hat{\mathbf{r}}) f^*(\hat{\mathbf{r}}_B, -\hat{\mathbf{r}}) d\Omega}_{T4}, \quad (8)$$

with

$$L_1 = |\mathbf{r} - \mathbf{r}_A| - |\mathbf{r} - \mathbf{r}_B|, \quad (9)$$

$$L_2 = |\mathbf{r} - \mathbf{r}_A| - r - r_B, \quad (10)$$

$$L_3 = |\mathbf{r} - \mathbf{r}_B| - r - r_A. \quad (11)$$

The integrals in terms $T1-T3$ have an oscillatory integrand that we analyze using the stationary phase approximation. The stationary points of the integrals $T1-T3$ are derived in the Appendix. The stationary points are located in the plane of the receivers, the (x, z) plane for the used coordinate system, and are sketched in Fig. 3.

The term $T1$ has two stationary phase points, indicated with the labels $1A$ and $1B$ on opposite ends of the line through \mathbf{r}_A and \mathbf{r}_B . Physically, the stationary phase point $1A$

gives a direct wave that propagates to \mathbf{r}_B and then continues along a straight path to \mathbf{r}_A . As shown in the Appendix, the stationary phase contribution from this point to term $T1$ gives

$$T_{1A} = -\frac{i\rho^2}{8\pi k} \frac{\exp(ik|\mathbf{r}_B - \mathbf{r}_A|)}{|\mathbf{r}_B - \mathbf{r}_A|} = \frac{i\rho}{2k} G_0(\mathbf{r}_A, \mathbf{r}_B), \quad (12)$$

where G_0 is the Green's function of the homogeneous medium in which the scatterer is embedded. The stationary phase point $1B$ gives after integration a direct wave that propagates in the opposite direction; it follows by interchanging the indices A and B and taking the complex conjugate of the contribution from point $1A$ as follows:

$$T_{1B} = -\frac{i\rho}{2k} G_0^*(\mathbf{r}_B, \mathbf{r}_A). \quad (13)$$

The stationary point 2A from term $T2$ corresponds to the correlation of a direct wave that propagates to \mathbf{r}_A with the scattered wave that arrives at \mathbf{r}_B . As shown in the Appendix, the contribution of this stationary phase point gives

$$T_{2A} = \frac{i\rho^2 \exp[-ik(r_A + r_B)]}{8\pi k r_A r_B} f^*(\hat{\mathbf{r}}_B, -\hat{\mathbf{r}}_A) = -\frac{i\rho}{2k} G_S^*(\mathbf{r}_B, \mathbf{r}_A). \quad (14)$$

This term accounts for the complex conjugate of the scattered wave G_S that propagates between the points \mathbf{r}_B and \mathbf{r}_A .

The stationary phase point 2B of term $T2$ gives the correlation between the direct wave arriving from that point at location \mathbf{r}_A and a scattered wave that propagates from the stationary phase point 2B through the scatterer to \mathbf{r}_B . As shown in the Appendix, the contribution of this stationary phase point is given by

$$T_{2B} = -\frac{i\rho^2 \exp[ik(r_A - r_B)]}{8\pi k r_A r_B} f^*(\hat{\mathbf{r}}_B, \hat{\mathbf{r}}_A). \quad (15)$$

This term is not a physical arrival because there is no wave that arrives with a phase given by the length difference $r_A - r_B$. Note that the phase of this term is identical to the phase of the spurious arrival $T4$ in Eq. (8).

The contribution of term $T3$ is due to the stationary points 3A and 3B in Fig. 3 that have the same physical interpretation as the stationary phase contribution of the points 2A and 2B, respectively, for term $T2$. Term $T3$ follows most simply by interchanging A and B in term $T2$ and by taking the complex conjugate. It thus follows from expressions (14) and (15) that

$$T3 = \frac{i\rho}{2k} G_S(\mathbf{r}_A, \mathbf{r}_B) + \frac{i\rho^2 \exp[ik(r_A - r_B)]}{8\pi k r_A r_B} f(\hat{\mathbf{r}}_A, \hat{\mathbf{r}}_B). \quad (16)$$

Taking all contributions into account by summing expressions (12)–(16) with term $T4$ from Eq. (8), and replacing the integration variable $\hat{\mathbf{r}}$ by $-\hat{\mathbf{r}}$ gives

$$\begin{aligned} & \oint G(\mathbf{r}_A, \mathbf{r}) G^*(\mathbf{r}_B, \mathbf{r}) d\Omega \\ &= -\frac{\rho}{2ik} [G(\mathbf{r}_A, \mathbf{r}_B) - G^*(\mathbf{r}_B, \mathbf{r}_A)] \\ &+ \frac{\rho^2 \exp[ik(r_A - r_B)]}{4\pi k r_A r_B} \left[-\frac{1}{2i} [f(\hat{\mathbf{r}}_A, \hat{\mathbf{r}}_B) - f^*(\hat{\mathbf{r}}_B, \hat{\mathbf{r}}_A)] \right. \\ &\left. + \frac{k}{4\pi} \oint f(\hat{\mathbf{r}}_A, \hat{\mathbf{r}}) f^*(\hat{\mathbf{r}}_B, \hat{\mathbf{r}}) d\Omega \right], \quad (17) \end{aligned}$$

where $G = G_0 + G_S$ is the sum of the direct and scattered waves.

The last term in expression (17) contains the spurious event discussed in Sec. II that does not correspond to a physical arrival. Perhaps surprisingly, there are two terms within the square brackets that arise from different stationary-phase arrivals from the different terms in the cross correlation. For this spurious arrival to cancel, and to make

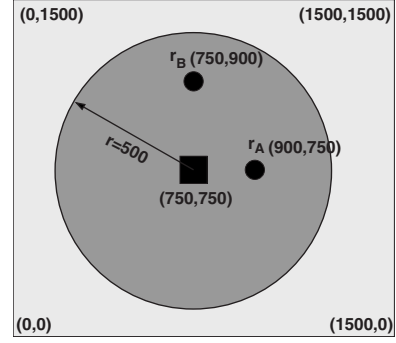


FIG. 4. Geometry of the numerical example. The 720 sources are located on a circle with radius 500 m. The scatterer in the origin has dimensions 10×10 m and is not shown to scale. All dimensions are in meters.

expression (17) equal to the general relation (2), the terms within the square brackets must vanish, hence

$$\frac{1}{2i} [f(\hat{\mathbf{r}}_A, \hat{\mathbf{r}}_B) - f^*(\hat{\mathbf{r}}_B, \hat{\mathbf{r}}_A)] = \frac{k}{4\pi} \oint f(\hat{\mathbf{r}}_A, \hat{\mathbf{r}}) f^*(\hat{\mathbf{r}}_B, \hat{\mathbf{r}}) d\Omega. \quad (18)$$

This relation is known as the *generalized optical theorem* that was derived earlier in quantum mechanics [23–25] and in acoustics [26]. This theorem guarantees that the spurious arrivals in expression (17) cancel.

IV. NUMERICAL EXAMPLE

We illustrate the cancellation of the spurious arrival with a numerical example based on the spectral-element method. This is a high-order variational numerical technique [27,28] that combines the flexibility of the finite-element method with the accuracy of global pseudospectral techniques. Widely used in seismology [29,30], we use the spectral-element method to simulate wave propagation in an acoustic model that contains an isolated scatterer.

The numerical example is in two dimensions, but it shows the same behavior as the theory derived above for three dimensions. The background velocity and density of the 1500×1500 m model are 1000 kg/m^3 and 1500 m/s , respectively, and a single square scatterer (10×10 m) is located in the origin. This scatterer has a velocity of 3000 m/s and a density of 2000 kg/m^3 . 720 sources are distributed evenly on a circle with a radius of 500 m from the center of the scatterer. The source wavelet is a Ricker wavelet with a central frequency of 50 Hz. In the spectral-element method, we use Lagrange polynomials of degree $N=4$ to interpolate the wave field in each quadrangular cell; the total number of spectral elements is 90 601. The time step used in the explicit integration scheme is $\Delta t=0.1$ ms and we propagate the signal for 0.53 s. The wave field is recorded at two receivers $\mathbf{r}_A=(900, 750)$ and $\mathbf{r}_B=(750, 950)$. The geometry of the experiment is drawn in Fig. 4, indicating that $G(\mathbf{r}_A, \mathbf{r}_B)$ contains a direct arrival at $t \approx 0.17$ s, and a scattered event at ≈ 0.23 s.

The top panel of Fig. 5 contains the cross correlations of the waves recorded at \mathbf{r}_B with those recorded at \mathbf{r}_A , for each

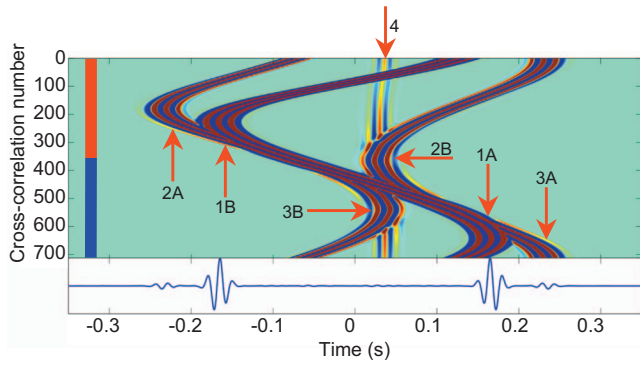


FIG. 5. (Color) Top panel: cross correlation of the waves recorded at the receivers as a function of time (horizontal axis) and source number (vertical axis) where the sources are numbered counterclockwise from the east. The labels at the stationary points are the same as in Fig. 3. The color bar on the left side in the upper panel indicates the subsets of sources used in Fig. 6. Bottom panel: the cross correlations after summation over all sources.

source. The bottom panel displays the sum of the cross correlations over all sources, i.e., it is the vertical sum of the waves in the top panel. The sinusoidal features in the top panel are the causal and acausal direct and scattered events with stationary points around $t \approx \pm 0.17$ s, and $t \approx \pm 0.23$ s, respectively. For example, the stationary point 1A gives the causal direct wave arriving at $t \approx 0.17$ s, while the stationary point 1B gives the acausal direct wave at $t \approx -0.17$ s. Similarly, the stationary points 2A and 3A give the causal and acausal scattered waves arriving at $t \approx \pm 0.23$ s. Of special interest is the arrival, marked with the label “4” at a travel time of about 0.03 s. Note that because of the finite size of the scatterer the arrival time of this wave is not quite constant, but it is the spurious arrival because it arrives before the direct wave. This spurious arrival is canceled by the contribution of the stationary points 2B and 3B. Indeed, there is no spurious arrival in the bottom panel at arrival time 0.03 s.

This numerical example confirms that the spurious arrival vanishes because of the destructive interference of the wave with nearly constant arrival time (marked with the label 4) with two stationary phase contributions 2B and 3B. Note that in this example we did not specify the scattering amplitude $f_k(\hat{\mathbf{n}}, \hat{\mathbf{n}}')$. Its properties are implicitly accounted for by the spectral element code.

In Fig. 6 we show the sum (in red) over the sources located along the lower half of the circle, and the sum (in blue) over the sources in the upper half circle. The sources along the lower half circle show the causal direct wave at $t \approx 0.17$ s and the causal scattered wave at $t \approx 0.23$ s, but not their acausal counterparts. The reason is that the sources on the lower half circle only launch direct and scattered waves that propagate from receiver A to receiver B. The sources along the upper half circle launch waves in the reverse direction, and give the acausal direct and scattered waves shown in blue. The spurious arrival is marked with the label “S.” Both subsets of sources give a nonzero spurious arrival. The contribution from the sources at the lower half mostly contribute to the nearly constant-time arrival marked with 4 in Fig. 5, while the sources from the lower half mostly con-

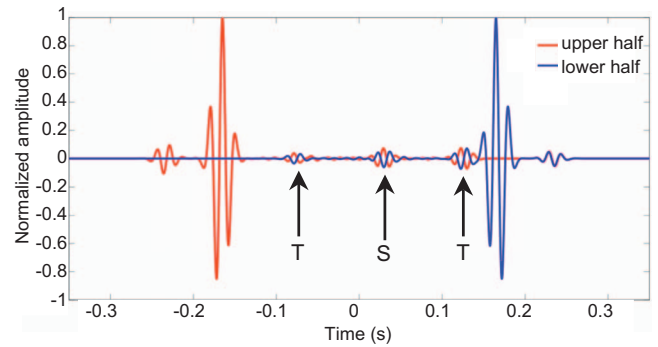


FIG. 6. (Color) The cross correlations of Fig. 5. Solid (red) trace: sum over all the sources along the lower half circle. Dashed (blue) trace: sum over the sources along the upper half circle. The spurious arrival is marked with the label “S,” while truncation phases are marked with the label “T.”

tribute to the stationary phase points 2B and 3B in Fig. 5. As shown in Fig. 6, each of these contributions is nonzero, but they do cancel when summed. The abrupt truncation of the sum over sources leads to additional truncation phases marked with “T,” that individually are nonzero, but whose sum vanishes as well. Truncation phases result from the dominant end-point contributions of oscillatory integrals [31], and are a known complication in modeling wave forms with the reflectivity method [32]. Truncation phases also occurred in field application of the extraction of the Green’s function from ocean-bottom seismic data [33]. Note that the arrival time of the truncation phases depends on the employed sources, while the arrival time of the spurious arrival is fairly constant for every truncated source distribution. Also, the truncated phases can be suppressed by suitable tapering of the source strength, but this does not suppress the spurious arrival.

V. CONCLUSION

This theoretical and numerical treatise of Green’s function retrieval in the presence of scattering has three implications. First, the comparison of expressions (2) and (17) shows that the generalized optical theorem holds. This work thus constitutes an alternative derivation of the generalized optical theorem, although Heisenberg’s original derivation [23], which was based on the unitary of the scattering matrix, is much simpler.

The second implication of this work is that, as shown in Fig. 6, for a limited source aperture the spurious arrivals do not vanish. Elegant proofs show that for a spherical scatterer in an elastic medium the exact Green’s function can be retrieved by cross correlation, provided that incident waves illuminate the scatterer with equal power from all directions [34,35]. It has been shown for a homogeneous medium [36] and for a layered medium [37] that spurious arrivals arise in the extracted Green’s function when the source aperture is limited. In seismic applications and other imaging problems, such spurious arrivals could be misinterpreted as scatterers or reflectors that are in reality not present. One should be aware of these spurious arrivals whenever the source distribution

used for the extraction of the Green's function does not fulfill theoretical requirements.

Third, it has been shown that both the correlation and deconvolution of waves recorded at different sensors leads to a new wave state that satisfies the same wave equation as the original system, albeit possible with different boundary and/or initial conditions [38]. As we show in this work, that wave state is for a limited illumination not necessarily the true Green's function, but the spurious arrivals that arise after cross correlation do carry information about the medium. Suppose, for example, that one wants to locate a scatterer in an application of target identification and location. Measuring the scattered waves, as in radar applications, constrains the distance $r_A + r_B$ traveled by the scattered wave. This constrains the scatterer to be located on an ellipsoid. In the numerical example, the spurious arrival is clearly visible. Such an arrival can be used to constrain the difference $r_A - r_B$, which constrains the scatterer to be located on a hyperboloid as well. Combining this complementary information makes it possible to locate the scatterer with greater accuracy. Correlation techniques applied to fields excited by an uneven source distribution do not necessarily produce the exact Green's function, but the extracted field does satisfy the underlying wave equation, and the spurious waves can glean information about the medium that is complementary to the direct and scattered waves.

ACKNOWLEDGMENTS

We are grateful for the critical and constructive remarks of the anonymous reviewers. We thank Dimitri Komatitsch and Jeroen Tromp for their spectral-element codes and for instructing us in their use. This work was partially supported by the National Science Foundation through Grant No. EAS-0609595 and by the US Geological Survey Mendenhall program.

APPENDIX: EVALUATION OF THE STATIONARY PHASE INTEGRALS

This section features details of the various stationary phase integrations starting with term $T1$ in Eq. (8). Using the vectors in expression (6), the length L_1 of Eq. (9) is given by

$$L_1 = \cos \varphi \sin \theta (r_B \sin \theta_B - r_A \sin \theta_A) + \cos \theta (r_B \cos \theta_B - r_A \sin \theta_A) = (x_B - x_A) \cos \varphi \sin \theta + (z_B - z_A) \cos \theta. \quad (\text{A1})$$

The integration is over the angles θ and φ and the stationary points are determined by the conditions

$$\frac{\partial L_1}{\partial \varphi} = -(x_B - x_A) \sin \varphi \sin \theta = 0, \quad (\text{A2})$$

$$\frac{\partial L_1}{\partial \theta} = (x_B - x_A) \cos \varphi \cos \theta - (z_B - z_A) \sin \theta = 0. \quad (\text{A3})$$

These expressions determine the angles θ_s and φ_s for which the phase of term $T1$ is stationary. The first condition gives

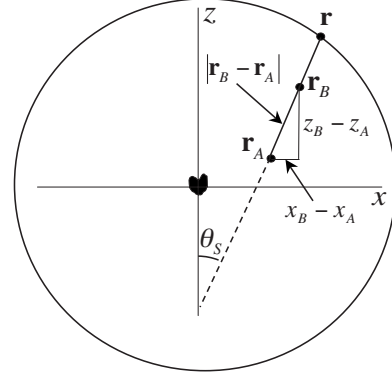


FIG. 7. Geometric variables for the stationary phase analysis of term $T1_A$.

$\sin \varphi_s = 0$, hence the stationary points are located in the (x, z) plane.

In the following we treat the stationary point $\varphi_s = 0$; the contribution of the stationary point $\varphi_s = \pi$ follows by complex conjugation. For $\varphi_s = 0$, expression (A3) gives

$$\tan \theta_s = \frac{x_B - x_A}{z_B - z_A}. \quad (\text{A4})$$

This angle is depicted in Fig. 7 where it can be seen that the stationary phase point is aligned with the points \mathbf{r}_A and \mathbf{r}_B .

Differentiation of expression (A3), and using the geometry of Fig. 7, gives for the second derivative at the stationary phase point

$$\begin{aligned} \frac{\partial^2 L_1}{\partial \theta^2} &= -(x_B - x_A) \sin \theta_s - (z_B - z_A) \cos \theta_s \\ &= -(x_B - x_A) \frac{x_B - x_A}{|\mathbf{r}_B - \mathbf{r}_A|} - (z_B - z_A) \frac{z_B - z_A}{|\mathbf{r}_B - \mathbf{r}_A|} \\ &= -|\mathbf{r}_B - \mathbf{r}_A|. \end{aligned} \quad (\text{A5})$$

Differentiation of expression (A2) gives at the stationary point

$$\frac{\partial^2 L_1}{\partial \varphi^2} = -(x_B - x_A) \sin \theta_s. \quad (\text{A6})$$

For this stationary term, and all other terms, the mixed derivative vanishes at the stationary phase point as follows:

$$\frac{\partial^2 L_1}{\partial \theta \partial \varphi} = 0. \quad (\text{A7})$$

It follows from the geometry of Fig. 7 that at the stationary phase point.

$$L_1 = |\mathbf{r} - \mathbf{r}_A| - |\mathbf{r} - \mathbf{r}_B| = |\mathbf{r}_A - \mathbf{r}_B|. \quad (\text{A8})$$

The stationary phase approximation of the θ and φ integration applied to the term $T1$ of expression (8) gives [39,31]

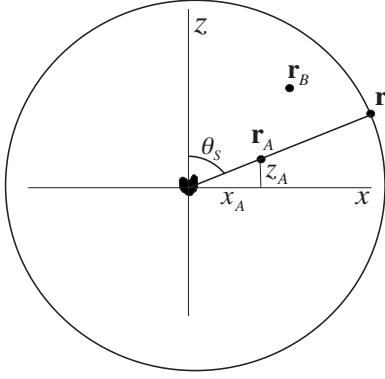


FIG. 8. Geometric variables for the stationary phase analysis of term T_{1A} .

$$T_{1A} = \frac{\rho^2}{(4\pi)^2} \exp(ik|\mathbf{r}_A - \mathbf{r}_B|) \times (e^{-i\pi/4})^2 \sqrt{\frac{2\pi}{k|\partial^2 L_1 / \partial \theta^2|}} \sqrt{\frac{2\pi}{k|\partial^2 L_1 / \partial \varphi^2|}} \sin \theta_s. \quad (\text{A9})$$

The factors $\exp(-i\pi/4)$ arise because the second derivatives both are negative. The $\sin \theta_s$ term comes from the Jacobian in the angular integration. With expressions (A5) and (A6) term T_{1A} reduces to

$$T_{1A} = -\frac{i\rho^2 \exp(ik|\mathbf{r}_A - \mathbf{r}_B|)}{8\pi k} \frac{\sin \theta_s}{\sqrt{|\mathbf{r}_A - \mathbf{r}_B|} \sqrt{\sin \theta_s |x_A - x_B|}}. \quad (\text{A10})$$

As shown in Fig. 7, $\sin \theta_s = (x_B - x_A) / |\mathbf{r}_A - \mathbf{r}_B|$. Inserting this in expression (A10) gives Eq. (12). Term T_{1B} in Eq. (13) follows by complex conjugation.

Next we treat the contribution of point 2A to term T_2 of expression (8). Using expression (6), the length L_2 is given by

$$L_2 = -r_A \cos \varphi \sin \theta \sin \theta_A - r_A \cos \theta \sin \theta_A - r_B \\ = -x_A \cos \varphi \sin \theta - z_A \cos \theta - r_B. \quad (\text{A11})$$

The stationary phase condition for the angle φ gives $\partial L_2 / \partial \varphi = x_A \sin \varphi \sin \theta = 0$, which implies that the stationary point lies in the (x, z) plane: $\sin \varphi_s = 0$. We first analyze the point $\varphi_s = 0$. For this point, the stationary phase condition for the variable θ is $\partial L_2 / \partial \theta = -x_A \cos \theta + z_A \sin \theta = 0$. This gives the stationary point

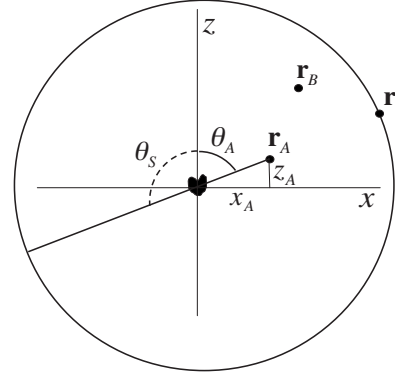


FIG. 9. Geometric variables for the stationary phase analysis of term T_{2B} .

$$\tan \theta_s = \frac{x_A}{z_A}. \quad (\text{A12})$$

This stationary phase point is sketched in Fig. 8. An analysis similar as for term T_1 shows that at this stationary point $L_2 = -r_A - r_B$, $\hat{\mathbf{r}} = -\hat{\mathbf{r}}_A$, $\partial^2 L_2 / \partial \theta^2 = r_A$, and $\partial^2 L_2 / \partial \varphi^2 = x_A \sin \theta_s$. The stationary phase contribution from point 2A to term T_2 of expression (8) thus is given by

$$T_{2A} = \frac{i\rho^2 \exp[-ik(r_A + r_B)]}{8\pi k} \frac{f^*(\hat{\mathbf{r}}_B, -\hat{\mathbf{r}}_A)}{r_B \sqrt{r_A}} \frac{\sin \theta_s}{\sqrt{\sin \theta_s x_A}}. \quad (\text{A13})$$

According to Fig. 8, $x_A = r_A \sin \theta_s$, which leads to expression (14).

The stationary phase point 2B corresponds to $\varphi_s = \pi$. The stationary phase condition for θ is in this case $\partial L_2 / \partial \theta = x_A \cos \theta + z_A \sin \theta = 0$. This gives the stationary point

$$\tan \theta_s = -\frac{x_A}{z_A}. \quad (\text{A14})$$

This point is sketched in Fig. 9. Using that $\theta_s = \pi - \theta_A$, it follows that at this stationary point $L_2 = r_A - r_B$, $\hat{\mathbf{r}} = \hat{\mathbf{r}}_A$, $\partial^2 L_2 / \partial \theta^2 = -r_A$, and $\partial^2 L_2 / \partial \varphi^2 = -x_A \sin \theta_A$. The stationary phase contribution of this point is thus given by

$$T_{2A} = -\frac{i\rho^2 \exp[ik(r_A - r_B)]}{8\pi k} \frac{f^*(\hat{\mathbf{r}}_B, \hat{\mathbf{r}}_A)}{r_B \sqrt{r_A}} \frac{\sin \theta_A}{\sqrt{\sin \theta_s x_A}}. \quad (\text{A15})$$

Using the geometric relation $\sin \theta_A = x_A / r_A$ reduces expression (A15) to Eq. (15).

- [1] A. Curtis, P. Gerstoft, H. Sato, R. Snieder, and K. Wapenaar, *The Leading Edge* **25**, 1082 (2006).
 [2] E. Larose, L. Margerin, A. Derode, B. van Tiggelen, M. Campillo, N. Shapiro, A. Paul, L. Stehly, and M. Tanter, *Geophysics* **71**, S111 (2006).
 [3] R. L. Weaver and O. I. Lobkis, *Phys. Rev. Lett.* **87**, 134301

(2001).

- [4] N. M. Shapiro, M. Campillo, L. Stehly, and M. H. Ritzwoller, *Science* **307**, 1615 (2005).
 [5] K. G. Sabra, P. Gerstoft, P. Roux, W. A. Kuperman, and M. C. Fehler, *Geophys. Res. Lett.* **32**, L14311 (2005).
 [6] K. G. Sabra, A. Srivastava, F. L. di Scalea, I. Bartoli, P. Rizzo,

- and S. Conti, *J. Acoust. Soc. Am.* **123**, EL8 (2008).
- [7] R. Snieder and E. Şafak, *Bull. Seismol. Soc. Am.* **96**, 586 (2006).
- [8] K. Mehta, R. Snieder, and V. Graizer, *Bull. Seismol. Soc. Am.* **97**, 1396 (2007).
- [9] M. Miyazawa, R. Snieder, and A. Venkataraman, *Geophysics* **75**, D35 (2008).
- [10] K. G. Sabra, S. Conti, P. Roux, and W. A. Kuperman, *Appl. Phys. Lett.* **90**, 194101 (2007).
- [11] A. Bakulin and R. Calvert, *Geophysics* **71**, SI139 (2006).
- [12] Kasper van Wijk, *Geophysics* **71**, SI79 (2006).
- [13] B. E. Hornby and J. Yu, *The Leading Edge* **26**, 760 (2007).
- [14] K. Wapenaar and J. Fokkema, *Geophysics* **71** SI33 (2006).
- [15] R. Snieder, K. Wapenaar, and U. Wegler, *Phys. Rev. E* **75**, 036103 (2007).
- [16] K. Wapenaar, J. Fokkema, and R. Snieder, *J. Acoust. Soc. Am.* **118**, 2783 (2005).
- [17] O. I. Lobkis and R. L. Weaver, *J. Acoust. Soc. Am.* **110**, 3011 (2001).
- [18] R. L. Weaver and O. I. Lobkis, *J. Acoust. Soc. Am.* **116**, 2731 (2004).
- [19] K. Wapenaar, E. Slob, and R. Snieder, *Phys. Rev. Lett.* **97**, 234301 (2006).
- [20] R. L. Weaver, *Wave Motion* **45**, 596 (2008).
- [21] P. M. Morse and K. U. Ingard, *Theoretical Acoustics* (McGraw-Hill, New York, 1968).
- [22] H. C. van de Hulst, *Physica (Amsterdam)* **15**, 740 (1949).
- [23] W. Heisenberg, *Z. Phys.* **120**, 513 (1943).
- [24] R. Glauber and V. Schomaker, *Phys. Rev.* **89**, 667 (1953).
- [25] L. I. Schiff, *Quantum Mechanics*, 3rd ed. (McGraw-Hill, New York, 1968).
- [26] P. L. Marsten, *J. Acoust. Soc. Am.* **109**, 1291 (2001).
- [27] E. Priolo, J. M. Carcione, and G. Seriani, *J. Acoust. Soc. Am.* **95**, 681 (1994).
- [28] E. Faccioli, F. Maggio, R. Paolucci, and A. Quarteroni, *J. Seismol.* **1**, 237 (1997).
- [29] D. Komatitsch and J. Tromp, *Geophys. J. Int.* **150**, 390 (2002).
- [30] D. Komatitsch, J. Ritsema, and J. Tromp, *Science* **298**, 1737 (2002).
- [31] C. M. Bender and S. A. Orszag, *Advanced Mathematical Methods for Scientists and Engineers* (McGraw-Hill, New York 1978).
- [32] L. J. Burdick and J. A. Orcutt, *Geophys. J. Int.* **58**, 261 (1979).
- [33] K. Mehta, R. Snieder, R. Calvert, and J. Sheiman, *The Leading Edge* **27**, 620 (2008).
- [34] F. J. Sánchez-Sesma, J. A. Pérez-Ruiz, M. Campillo, and F. Luzón, *Geophys. Res. Lett.* **33**, L13305 (2006).
- [35] F. J. Sánchez-Sesma and M. Campillo, *Bull. Seismol. Soc. Am.* **96**, 1182 (2006).
- [36] H. Nakahara, *Geophys. J. Int.* **167**, 1097 (2006).
- [37] R. Snieder, K. Wapenaar, and K. Larner, *Geophysics* **71**, SI111 (2006).
- [38] R. Snieder, J. Sheiman, and R. Calvert, *Phys. Rev. E* **73**, 066620 (2006).
- [39] N. Bleistein and R. A. Handelsman, *Asymptotic Expansions of Integrals* (Dover, New York, 1975).